SAGE-Hindawi Access to Research
International Journal of Electrochemistry
Volume 2011, Article ID 381960, 8 pages
doi:10.4061/2011/381960

Research Article

Influence of the C/Sn Ratio on the Synthesis and Lithium Electrochemical Insertion of Tin-Supported Graphite Materials Used as Anodes for Li-Ion Batteries

Cédric Mercier,[1] Raphaël Schneider,[2] Patrick Willmann,[3] and Denis Billaud[1]

[1] *Laboratoire de Chimie du Solide Minéral, Nancy-University, CNRS, BP 239, 54506 Vandoeuvre-les-Nancy Cedex, France*
[2] *Laboratoire Réactions et Génie des Procédés (LRGP), UPR 3349, Nancy-University, CNRS, 1 rue Grandville, 54001 Nancy Cedex, France*
[3] *Centre National d'Etudes Spatiales (CNES), 18 Avenue E. Belin, 31055 Toulouse Cedex, France*

Correspondence should be addressed to Denis Billaud, denis.billaud@lcsm.uhp-nancy.fr

Received 21 January 2011; Accepted 25 February 2011

Academic Editor: S. Gopukumar

Novel composites consisting of tin particles associated to graphite were prepared by chemical reduction of tin(+2) chloride by *t*-BuONa-activated sodium hydride in the presence of graphite. The samples obtained using various C/Sn ratios were investigated by X-ray powder diffraction (XRD), transmission electron microscopy (TEM), scanning electron microscopy (SEM), and elemental analyses. The largest tin particles associated to graphite layers were observed for the material with a C/Sn ratio of 16. For the materials with C/Sn ratios of 42 and 24, SEM and TEM experiments demonstrated that Sn aggregates of ca. 250 nm length and composed of Sn particles with an average diameter of ca. 50 nm were homogeneously distributed at the surface of graphite. Electrodes prepared from the C/Sn = 42 material exhibit a high reversible capacity of over 470 $mAhg^{-1}$ up to twenty cycles with stable cyclic performances.

1. Introduction

With the development of portable electronic devices and the enormous interest in the hybrid electric vehicle market, the demand for power sources with higher storage capacity, longer operating times, as well as safety, environmental compatibility, and low production costs has markedly increased [1].

Graphite is mainly used as negative electrode materials for lithium ion secondary batteries and yields a theoretical capacity of 372 $mAhg^{-1}$. Lithium alloys, which can be reversibly formed and decomposed electrochemically in nonaqueous electrolyte solutions, are natural alternative candidates to both lithium and lithiated graphite in rechargeable Li-based batteries. Of special importance in this respect are the lithium-tin compounds. Indeed, both metallic tin and tin oxide (SnO_2) were shown as interesting anode materials for Li-ion batteries because of their conducting properties combined with high specific capacities (Sn, 994 $mAhg^{-1}$ and SnO_2, 781 $mAhg^{-1}$) [2, 3] compared to that of graphite [4, 5]. Lithium can be inserted into tin to form alloys of high Li content up to $Li_{22}Sn_5$, corresponding to a theoretical capacity of 994 $mAhg^{-1}$ [2]. Although these attractive features have initiated a number of studies on Sn-based hosts [4, 6–19], Li^+ ion insertion/extraction into/from Sn causes volume changes [9, 20, 21]. These changes result in cracking and crumbling of the electrode with the concomitant loss of electrical contact both between interparticles, and between particles and the current collector, resulting in poor cycling performance.

A promising way of improving the cyclability of Sn-based electrodes is to synthesize small-sized Sn particles. We have recently developed a new method for the preparation of nanosized Sn particles based on the reduction of tin +2 or +4 chlorides by alkoxide-activated sodium hydride [14, 15]. The discharge capacity of graphite/Sn materials prepared by this method was maintained above ca. 420 $mAhg^{-1}$ after 15 cycles [16, 19].

In this paper, in order to study the effect of the C/Sn ratio on the electrochemical characteristics of the Sn negative electrode, tin-supported graphite materials were synthesized by reduction of $C/SnCl_2$ mixtures of various ratios (5, 8, and 12) using the *t*-BuONa-activated NaH chemical reduction process. The structural and morphological changes and electrochemical performances of the materials obtained were studied. All investigations were discussed with respect to unmodified graphite.

2. Experimental

2.1. Synthesis of Graphite/Sn Nanocomposites. The C/Sn materials were prepared by reduction of $SnCl_2$ by *t*-BuONa-activated NaH in anhydrous THF. Prior to the experiment, NaH was degreased by washing with anhydrous THF under protective nitrogen atmosphere. In a typical experiment, NaH (resp., 41, 61 or 97 mmol for initial C/Sn ratios of 12, 8, and 5) was dispersed in 25 mL THF and the mixture was heated at 65°C under vigorous stirring. *t*-BuOH (resp., 20, 30, or 48 mmol for C/Sn ratios of 12, 8, and 5) was then added dropwise to form the alkoxide-activated hydride *t*-BuONa/NaH. The stirring was continued for 15 min and the mixture was then cooled to room temperature. Graphite (1.44 g) was then added and the mixture was further stirred for 10 min. $SnCl_2$ (resp., 10, 15, or 24 mmol for C/Sn ratios of 12, 8, and 5) was then added in one portion and the mixture was heated to reflux under constant stirring for 1 h. Hydrogen gas release can be observed, indicating the reduction of $SnCl_2$ into Sn(0) nanoparticles as presented in

$$\mathrm{SnCl_2} + \mathrm{xC_{graphite}} + \frac{2\mathrm{NaH}}{t\text{-BuONa}} \xrightarrow{\mathrm{THF}} \frac{\mathrm{xC_{graphite}/Sn(0)}}{2t\text{-BuONa}} + \mathrm{H_2} + 2\mathrm{NaCl} \quad (1)$$

After the reaction had been stopped by cooling down the solution to room temperature, THF and organic volatiles were evaporated under vacuum (40°C, 10 mmHg). The dark grey powder obtained was first dried at room temperature overnight, washed with ethanol (2×30 mL) and water (2×30 mL) by centrifugation to remove NaCl, the stabilizing alkoxide *t*-BuONa, and unreacted starting materials, and finally dried in vacuum for 12 h (room temperature, 10^{-3} mmHg).

2.2. Materials Characterization. Powder (XRD) analyses were carried out using an automated powder diffractometer with MoKα radiation (λ = 0.709 Å) (Rotaflex RU-200B, RIGAKU generator and CPS 120 INEL detector, transmission assembly) in capillary mode. Powder was introduced under argon into Lindemann tubes which were further sealed to avoid any pollution. Transmission electron microscopy (TEM) images were taken by placing a drop of the particles in THF onto a carbon film supported copper grid. Samples were studied using a Philips CM20 instrument with LaB_6 cathode operating at 200 kV and equipped with an EDX (EDAX) spectrometer. A field emission gun-scanning electron microscopy (FEG-SEM Hitachi S2500) equipped with EDX analysis was also used.

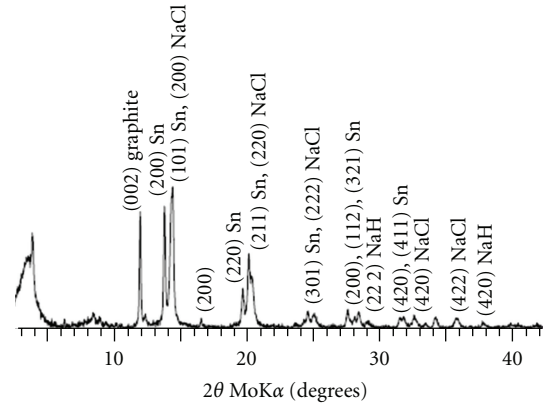

Figure 1: XRD patterns of the material prepared with a C/Sn ratio of 8 after synthesis and drying.

2.3. Electrochemical Measurements. Electrochemical tests were carried out in half cells with lithium acting both as reference and counter electrode in 1.5 M $LiClO_4$-ethylene carbonate (EC). The working electrode was made by coating a 1-methyl-2-pyrrolidinone slurry of 90% w/w of the Sn-based material and 10% w/w of polyvinylidene fluoride (PVDF) on a copper current collector. Charge and discharge cycles were monitored in galvanostatic mode using a Mac Pile potentiostat-galvanostat (Biologic). The output voltage was recorded for a specific current cell of 10 μA/mg applied for 6 min followed by a 10 s relaxation period.

3. Results and Discussion

3.1. Structure of the C/Sn Materials. In order to gain insights into the chemical composition and into the atomic ratio of Sn/C in the composites after purification, as-prepared and washed samples were first submitted to elemental analyses. For the as-prepared materials and after subtraction of the carbon associated to the stabilizing *t*-BuONa alkoxide, chemical analyses afforded C/Sn ratios in good accordance with those expected when starting with initial C/Sn ratios of 12, 8, and 5. The atomic percentage of tin removed during the washing process was found to be high, quite 70% for the 3 composites prepared. After washing, C/Sn ratios determined by elemental analyses were of 42, 24, and 16, respectively, for materials prepared with initial C/Sn ratios of 12, 8, and 5 (Table 1).

The phase and purity of the powder samples prepared were first determined by X-ray diffraction (XRD). A typical diffraction pattern of the material prepared with a C/Sn ratio of 8 before washing is shown in Figure 1. For the as-synthesized nanocomposite, the diffraction peaks at low angles (<10°) were characteristic of the organic *t*-BuONa matrix used to stabilize the tin nanoparticles [22]. All the other reflections of the crude sample could be readily

Table 1: Reversible theoretical and experimental capacities of the C/Sn = 42, C/Sn = 24, and C/Sn = 16 nanocomposites.

Materials composition			Reversible capacities calculated from elemental analyses ($mAhg^{-1}$)			Reversible capacities calculated from electrochemical curves ($mAhg^{-1}$)		
Initial C/Sn ratio	Experimental C/Sn ratio[a]		Total	Graphite	Tin	Total	Graphite	Tin
12	42	Cycle 1	453	279	175	455	285	170
		Cycle 20	453	279	175	478	321	157
8	24	Cycle 1	497	260	237	430	228	202
		Cycle 20	497	260	237	420	240	180
5	16	Cycle 1	550	208	342	450	243	207
		Cycle 20	550	208	342	428	245	182

[a]Determined from elemental analysis.

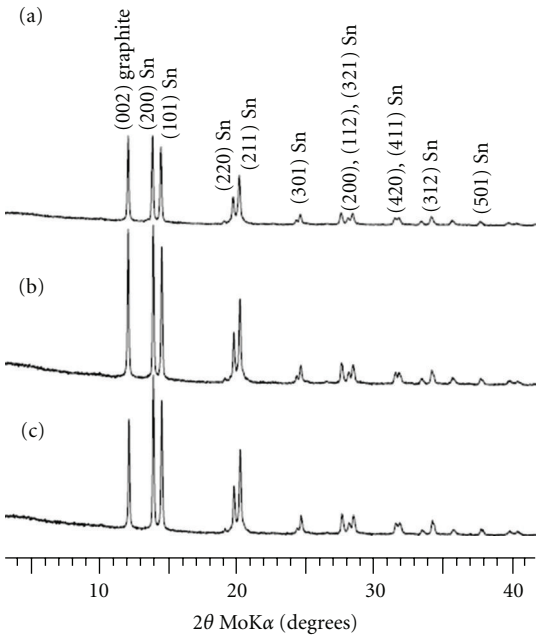

Figure 2: XRD patterns of the nanocomposites with C/Sn ratios of (a) 42, (B) 24, and (c) 16, after washing with ethanol and water and drying.

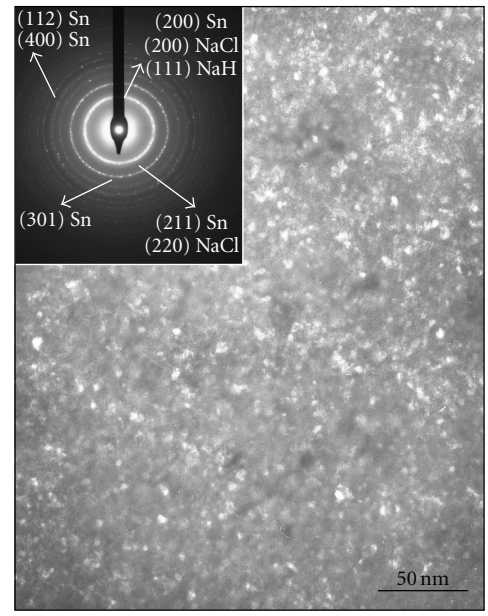

Figure 3: Typical TEM micrograph of the as-prepared graphite/tin nanocomposites before washing. The inset is the selected area electron diffraction of the material showing crystalline characteristics of β-Sn.

assigned to metallic β-Sn (JCPDS No 04-0673) and to sodium chloride, present as a byproduct of the reduction. For β-Sn, all reflections correspond to the $I4_1/amd$ space group (a = b = 5.831 Å, c = 3.182 Å, $\alpha = \beta = \gamma = 90°$). A small peak at around 16.8° can be associated to the residual sodium hydride in the crude reaction product.

Peaks related to sodium chloride, sodium hydride, and to the organic matrix disappeared after washing with ethanol and water, and the final nanocomposites with C/Sn ratios of 42, 24, and 16 showed only the reflections of β-Sn and of graphite (strong (002) diffraction line, d_{002}, at ca. 12°) (Figure 2). No crystalline impurities related to reaction by-products or to crystalline tin oxides were detected for the powders after washing.

Further investigations of Sn/graphite nanocomposites were performed by transmission electron microscopy (TEM) and scanning electron microscopy (SEM). Using TEM, it was observed that Sn particles obtained after synthesis and drying have sizes well below 10 nm (Figure 3). They are spherically shaped, show a homogeneous distribution with an average diameter of 5.5 nm, and exhibit the diffraction rings of β-Sn.

Upon washing with ethanol and water, nanometer-sized Sn particles coalesce and aggregate into larger particles due to the removal of the stabilizing *t*-BuONa ligand. Regardless of the C/Sn ratio, TEM micrographs (Figures 4(a)–4(c)) show that Sn is present as aggregates (with lengths up to 250 nm) composed of spherical particles with diameters ranging from 10 to 50 nm. The corresponding selected-area electron diffraction (SAED) patterns show clear ring patterns confirming the formation of polycrystalline C/Sn materials. The diffraction rings from inside to the outside of the pattern can be indexed to the (200), (101), (220), (321), (312), and (521) planes of quadratic β-Sn, respectively. These results are in good accordance with those of the previous XRD studies.

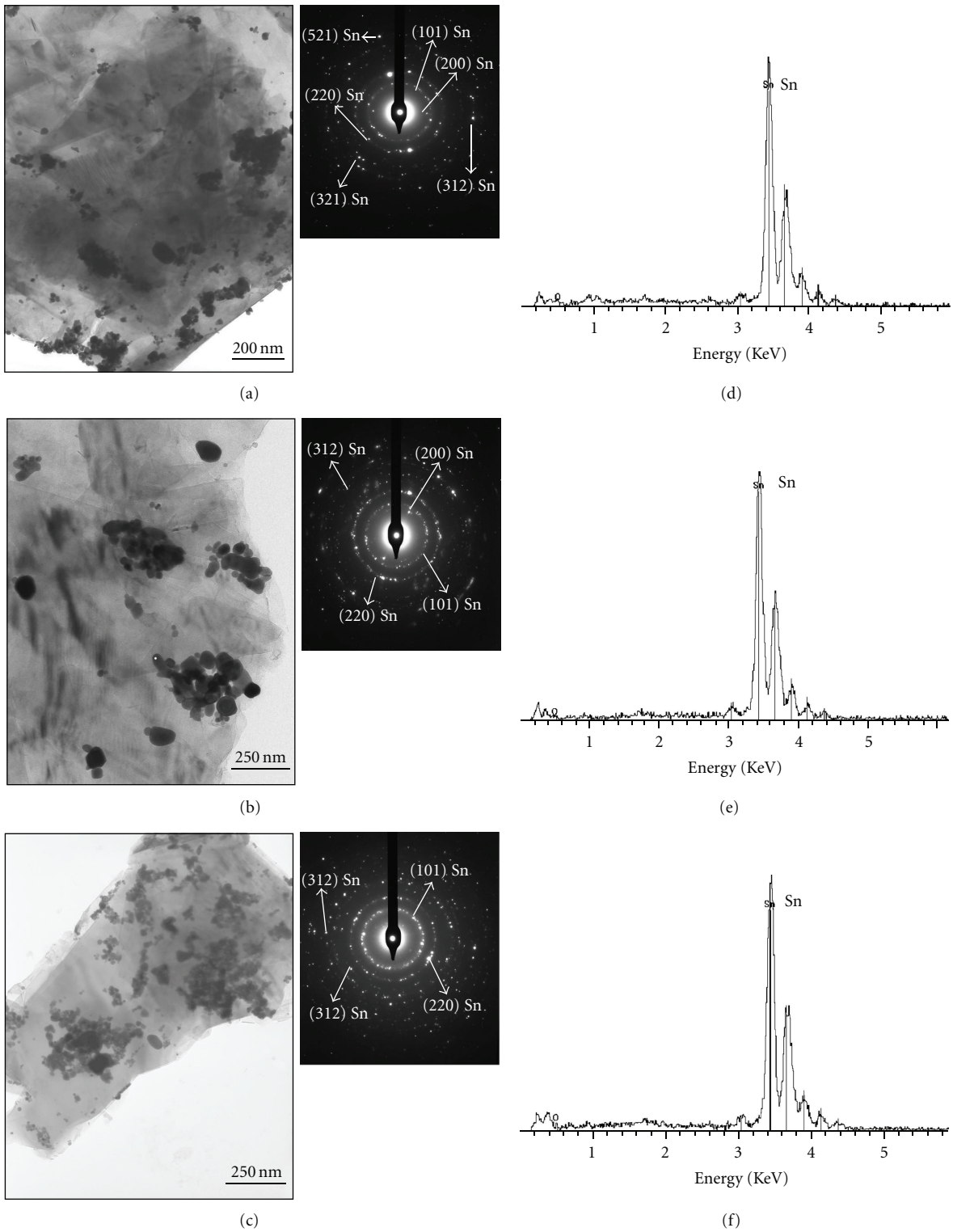

Figure 4: TEM images, selected area electron diffraction patterns (SAED), and associated EDS spectra of Sn/graphite nanocomposites after washing with ethanol and water. (a) and (d) C/Sn = 42; (b) and (e) C/Sn = 24; (c) and (f) C/Sn = 16.

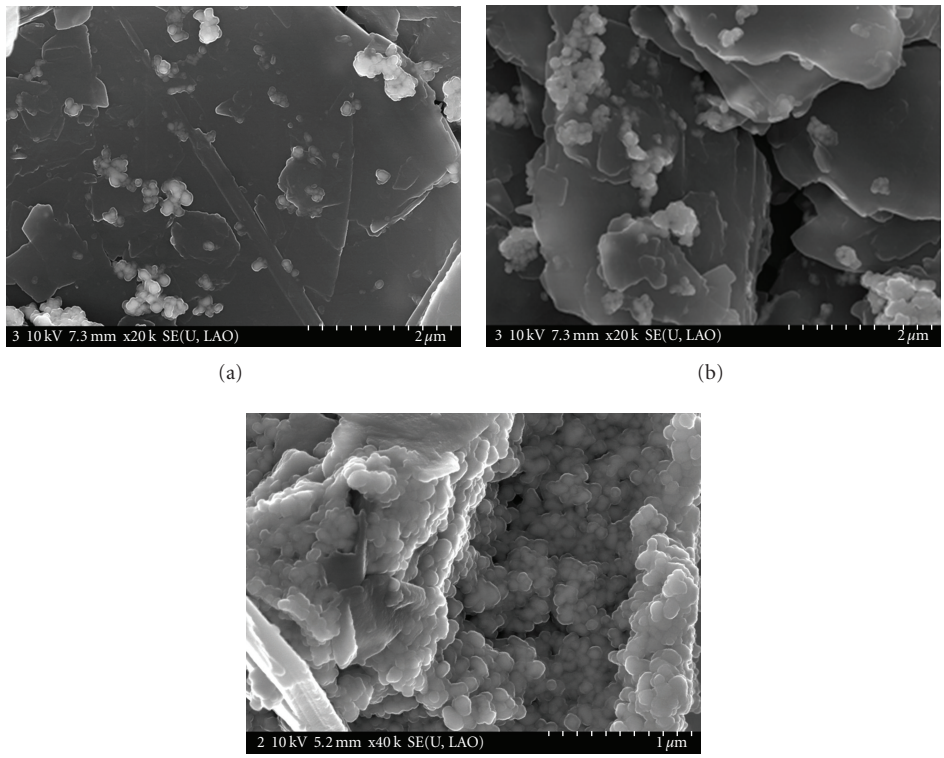

Figure 5: SEM micrographs of the Sn/graphite nanocomposites; (a) C/Sn = 42, (b) C/Sn = 24, and (c) C/Sn = 16.

The energy dispersive X-ray spectra (EDX) depicted in Figures 4(d)–4(f) performed on particles aggregates suggest the existence of Sn and O in the washed materials. Elemental analyses derived from EDX spectra show that the weight percentage of O associated to Sn varies between 0 and 7% depending on the particles observed. Using TEM, it was finally observed that Sn particles are located at the edge of graphite layers and at the surface of graphite regardless of the nanocomposite.

Scanning electron microscopy (SEM) observations confirmed the microstructure of Sn particles after purification (Figure 5). All composites contain large Sn aggregates (up to 300 nm) composed of smaller Sn particles possessing an average diameter of ca. 50 nm, which is in accordance with TEM observations. The amount of agglomerated Sn increased with the content of metal in the composite material. Large aggregates with lengths up to 4 μm nonhomogeneously distributed at the surface of graphite layers could clearly be observed for the material with a C/Sn ratio of 16 (Figure 5(c)). Graphite layers provide a limited number of active surface sites for Sn particles anchorage. The formation of the large particles for the C/Sn = 16 material could be a consequence of the high metal content of this composite where metal particles are not adequately stabilized.

3.2. Electrochemical Properties of the C/Sn Materials. To evaluate the potential applicability in Li-ion batteries, we investigated some electrochemical characterizations of the Sn/graphite composites with respect to Li insertion/extraction. Figure 6 shows a comparison of the voltage profiles of C/Sn washed materials with C/Sn ratios of 42, 24, and 16. Figure 7 and Table 1 summarize the reversible and irreversible theoretical and experimental capacities of the 3 samples.

For the C/Sn = 42 material, the full capacity is of 1145 $mAh \cdot g^{-1}$ during the first reduction. 700 $mAh \cdot g^{-1}$ are due to irreversible losses related to the reduction of the tin oxidized species and to the formation of the Solid Electrolyte Interphase (SEI) passivation layer at the surface of graphite and on tin particles. Tin oxides SnO and SnO_2 are reduced between 1.8 V and 1.5 V versus Li^+/Li, respectively. One observes on the first cycle a beginning of reduction towards 1.8 V which continues until 0.8 V and which extends on a relatively large range of capacities (approximately 220 $mAh \cdot g^{-1}$). The reduction of tin oxides (Sn^{+4}, Sn^{+2} were evidenced by recent Mossbauer studies [23]) present in our composite can thus be estimated to be ca. 10 $mAh \cdot g^{-1}$. Side reactions with products composing the matrix surrounding the Sn nanoparticles should also be considered taking into account that the composite contains ca. 7.5 wt% of these materials according to elemental analysis. Around 0.8–0.6 V versus Li^+/Li, the formation of the passivation layer (reduction of electrolytic species) occurs. The insoluble products thus generated precipitate at the surface of graphite and tin nanoparticles forming an impermeable film to the solvent molecules but allowing the diffusion of Li^+ cations. The irreversible capacity related to graphite during

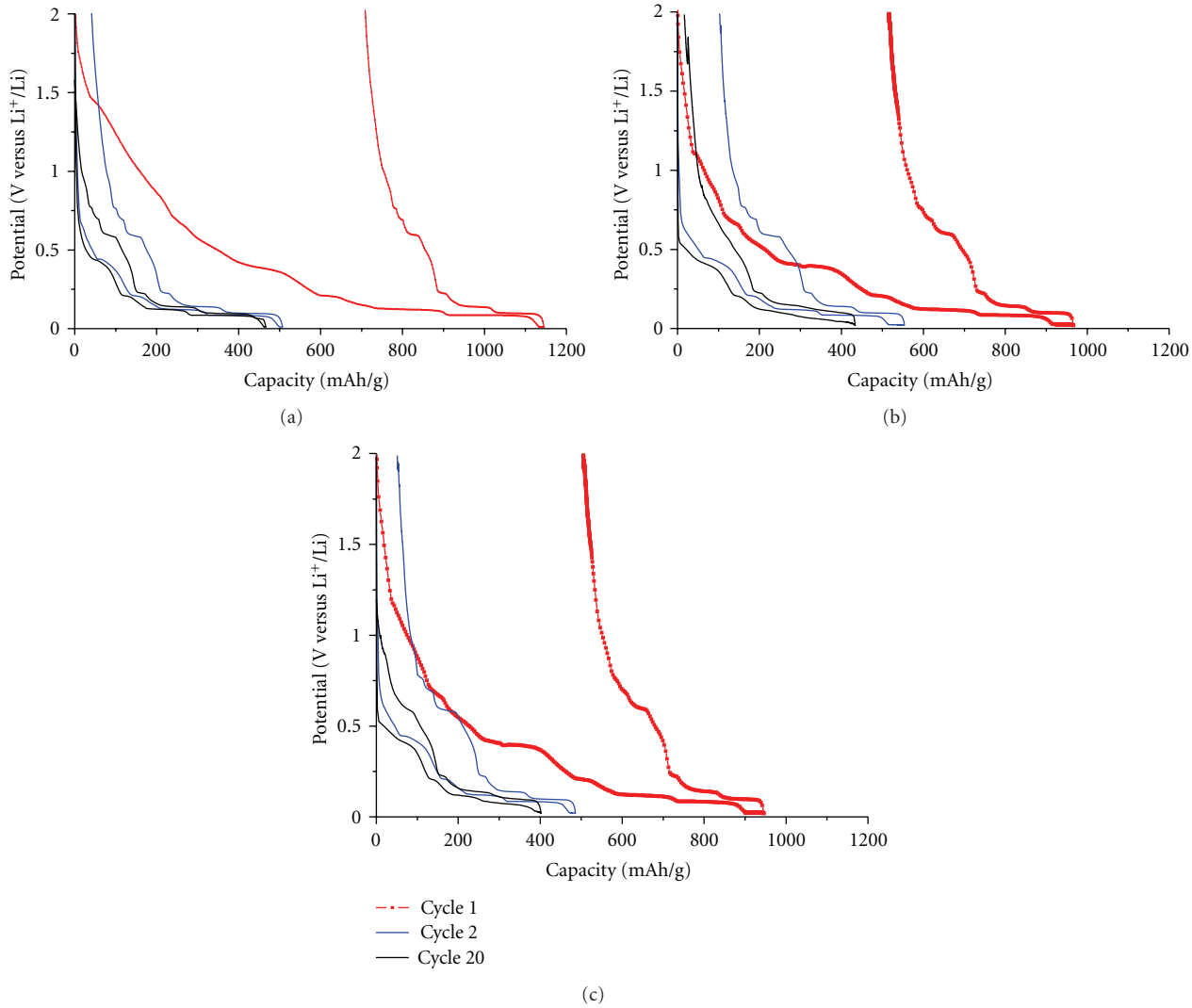

FIGURE 6: Voltage profiles of the (a) C/Sn = 42, (b) C/Sn = 24, and (c) C/Sn = 16 materials cycled between 0 and 2.0 V. The 1rst, 2nd, and 20th cycles have been reported for further comparison.

the formation of this passivation layer can be estimated to be ca. 100 mAh·g^{-1}. The 380 mAh·g^{-1} remaining can form the SEI on tin. The irreversible capacity decreases very quickly (30 mAh·g^{-1} at the second cycle) and disappears at the third cycle.

At the first cycle, the reversible capacity is 455 mAh·g^{-1}, in which 285 mAh·g^{-1} can be attributed to graphite and 170 mAh·g^{-1} are related to tin. In the second cycle, the reversible capacity increases notably and reaches 478 mAh·g^{-1} (321 mAh·g^{-1} for graphite and 157 mAh·g^{-1} for tin). This reversible capacity remains stable until the 20th cycle. During the first two cycles, the reversible capacity related to graphite increases by 12% (from 285 to 321 mAh·g^{-1}). We suppose that, during the synthesis, graphite undergoes small structural disorders which prevent it from cycling at its maximal value during the first cycles. In the meantime, the reversible capacity related to tin decreases by 8% (from 170 to 157 mAh·g^{-1}). This decrease can originate from the loss of electrical contact between tin(0) particles formed by the reduction of the oxidized tin species during the first cycle. Indeed, these particles are surrounded by Li_2O, by-product of the reduction, which is a bad electronic conducting material [4, 24]. The formation of large particles and/or aggregates, which behave like massive tin, can also be hypothesized.

A theoretical reversible capacity can be calculated using the values obtained from elemental analyses. The value obtained is 453 mAh·g^{-1}, in which 279 mAh·g^{-1} can be attributed to UF_4 graphite and 175 mAh·g^{-1} related to tin. The values of experimental capacities related to graphite and tin suppose that there is no covering between the end and the beginning of the insertion of lithium in tin and graphite. Of course, actually there exists a small zone of potential where the two processes take place simultaneously. Thus the values indicated above for the share of reversible capacity related to tin and to graphite are very slightly underestimated for tin and on the contrary overestimated for graphite.

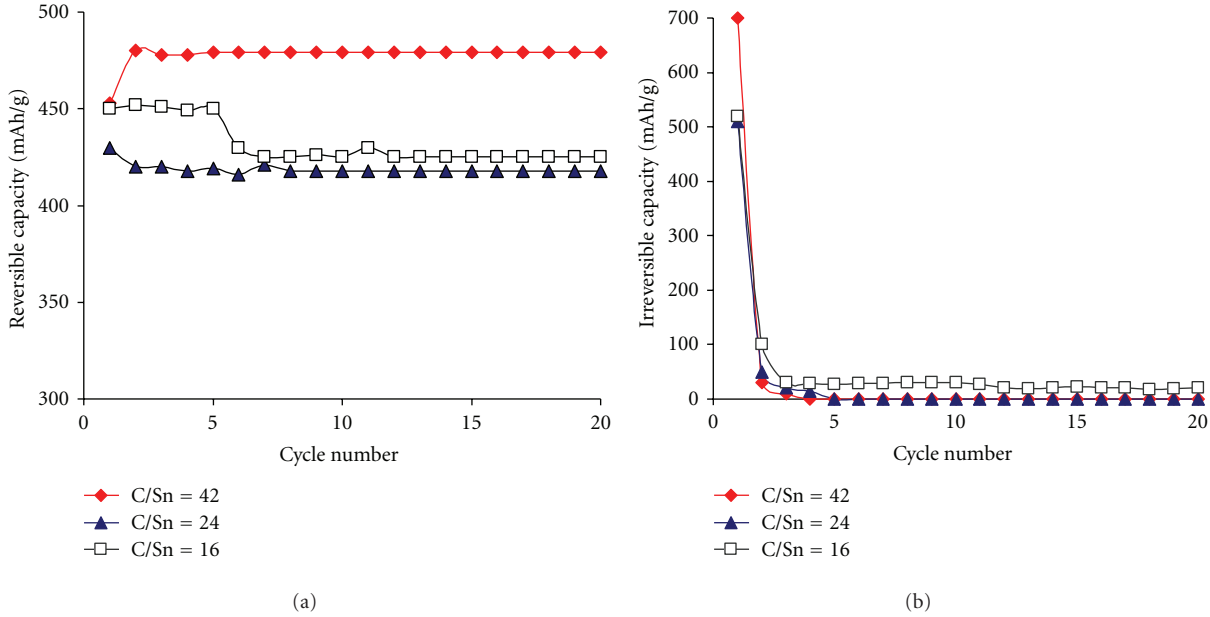

Figure 7: Evolution of (a) the reversible and (b) the irreversible capacities of the C/Sn = 42, C/Sn = 24, and C/Sn = 16 materials versus cycle number.

The electrochemical behaviour of the samples containing larger amounts of tin (C/Sn = 24 and C/Sn =16) is close to that obtained for the C/Sn = 48 material. One can however note that the reversible capacities are slightly lower throughout the 20 cycles and that irreversible capacities persist upon cycling around 30 $mAh \cdot g^{-1}$. Table 1 shows finally that during the first cycle, a considerable part of tin is electrically isolated and does not cycle (20% and 40%, respectively, for C/Sn = 24 and C/Sn = 16 nanocomposites, calculated using elemental analysis values and with the first cycle voltage profiles).

4. Conclusion

In summary, we have demonstrated that the solution phase reduction process using *t*-BuONa-activated NaH in THF can be successfully used for the preparation of tin particles dispersed on graphite. A comparison of the electrochemical behaviour of the materials obtained using C/Sn ratios of 42, 24, and 16 revealed that, despite the high irreversible capacity observed for the theoretical C/Sn = 42 nanocomposite at the first cycle, this material exhibits a high reversible capacity of ca. 480 $mAhg^{-1}$ over 20 cycles, that is higher by 37% than the practical expected for pure graphite (350 $mAhg^{-1}$). This result might be related to the improved dispersion of Sn nanoparticles at the surface of graphite in this composite compared to materials prepared with C/Sn ratios 24 or 16 as demonstrated by TEM and SEM characterizations. Our study shows that the C/Sn ratio used for the preparation of tin/graphite composites is of great importance for obtaining good cycling performances and thus for the development of Sn/graphite systems which could be used as anode materials for Li-ion batteries.

References

[1] J.-M. Tarascon and M. Armand, "Issues and challenges facing rechargeable lithium batteries," *Nature*, vol. 414, no. 6861, pp. 359–367, 2001.

[2] M. Winter and J. O. Besenhard, "Electrochemical lithiation of tin and tin-based intermetallics and composites," *Electrochimica Acta*, vol. 45, no. 1-2, pp. 31–50, 1999.

[3] G. Derrien, J. Hassoun, S. Panero, and B. Scrosati, "Nanostructured Sn-C composite as an advanced anode material in high-performance lithium-ion batteries," *Advanced Materials*, vol. 19, no. 17, pp. 2336–2340, 2007.

[4] Y. Idota, T. Kubota, A. Matsufuji, Y. Maekawa, and T. Miyasaka, "Tin-based amorphous oxide: a high-capacity lithium-ion-storage material," *Science*, vol. 276, no. 5317, pp. 1395–1397, 1997.

[5] E. Kim, D. Son, T.-G. Kim et al., "Mesoporous/crystalline composite material containing tin phosphate for use as the anode in lithium-ion batteries," *Angewandte Chemie International Edition*, vol. 43, no. 44, pp. 5987–5990, 2004.

[6] M. Winter, J. O. Besenhard, M. F. Spahr, and P. Novak, "Insertion electrode materials for rechargeable lithium batteries," *Advanced Materials*, vol. 10, no. 10, pp. 725–763, 1998.

[7] R. A. Huggins, "Lithium alloy negative electrodes," *Journal of Power Sources*, vol. 81-82, no. 1-2, pp. 13–19, 1999.

[8] J. Yang, M. Wachtler, M. Winter, and J. O. Besenhard, "Submicrocrystalline Sn and Sn-SnSb powders as lithium storage materials for lithium-ion batteries," *Electrochemical and Solid-State Letters*, vol. 2, no. 2–4, pp. 161–163, 1999.

[9] L. Y. Beaulieu, S. D. Beattie, T. D. Hatchard, and J. R. Dahn, "The electrochemical reaction of lithium with tin studied by in situ AFM," *Journal of the Electrochemical Society*, vol. 150, no. 4, pp. A419–A424, 2003.

[10] A. Trifonova, M. Winter, and J. O. Besenhard, "Structural and electrochemical characterization of tin-containing graphite compounds used as anodes for Li-ion batteries," *Journal of Power Sources*, vol. 174, no. 2, pp. 800–804, 2007.

[11] S.-H. Ng, S.-Y. Chew, D. I. Dos Santos et al., "Hexagonal-shaped tin glycolate particles: a preliminary study of their suitability as Li-ion insertion electrodes," *Chemistry—An Asian Journal*, vol. 3, no. 5, pp. 854–861, 2008.

[12] P. Meduri, C. Pendyala, V. Kumar, G. U. Sumanasekera, and M. K. Sunkara, "Hybrid tin oxide nanowires as stable and high capacity anodes for Li-ion batteries," *Nano Letters*, vol. 9, no. 2, pp. 612–616, 2009.

[13] K. Ui, S. Kikuchi, Y. Kadoma, N. Kumagai, and S. Ito, "Electrochemical characteristics of Sn film prepared by pulse electrodeposition method as negative electrode for lithium secondary batteries," *Journal of Power Sources*, vol. 189, no. 1, pp. 224–229, 2009.

[14] L. Balan, R. Schneider, D. Billaud, and J. Ghanbaja, "Novel low-temperature synthesis of tin(0) nanoparticles," *Materials Letters*, vol. 59, no. 8-9, pp. 1080–1084, 2005.

[15] L. Balan, R. Schneider, D. Billaud, and J. Ghanbaja, "A new organometallic synthesis of size-controlled tin(0) nanoparticles," *Nanotechnology*, vol. 16, no. 8, pp. 1153–1158, 2005.

[16] L. Balan, J. Ghanbaja, P. Willmann, and D. Billaud, "Novel tin-graphite composites as negative electrodes of Li-ion batteries," *Carbon*, vol. 43, no. 11, pp. 2311–2316, 2005.

[17] L. Balan, R. Schneider, J. Ghanbaja, P. Willmann, and D. Billaud, "Electrochemical lithiation of new graphite-nanosized tin particle materials obtained by $SnCl_2$ reduction in organic medium," *Electrochimica Acta*, vol. 51, no. 17, pp. 3385–3390, 2006.

[18] D. Billaud, L. Balan, R. Schneider, and P. Willmann, "The influence of the synthesis conditions of graphite/tin nanoparticle materials on their electrode electrochemical performance in Li-ion battery anodes," *Carbon*, vol. 44, no. 12, pp. 2508–2515, 2006.

[19] L. Balan, R. Schneider, P. Willmann, and D. Billaud, "Tin-graphite materials prepared by reduction of $SnCl_4$ in organic medium: synthesis, characterization and electrochemical lithiation," *Journal of Power Sources*, vol. 161, no. 1, pp. 587–593, 2006.

[20] I. A. Courtney and J. R. Dahn, "Electrochemical and in situ X-ray diffraction studies of the reaction of lithium with tin oxide composites," *Journal of the Electrochemical Society*, vol. 144, no. 6, pp. 2045–2052, 1997.

[21] A. Sivashanmugara, T. P. Kumar, N. G. Renganathan, S. Gopukumar, M. Wohlfahrt-Mehrens, and J. Garche, "Electrochemical behavior of Sn/SnO_2 mixtures for use as anode in lithium rechargeable batteries," *Journal of Power Sources*, vol. 144, no. 1, pp. 197–203, 2005.

[22] C. Nabais, R. Schneider, C. Bellouard, J. Lambert, P. Willmann, and D. Billaud, "A new method for the size- and shape-controlled synthesis of lead nanostructures," *Materials Chemistry and Physics*, vol. 117, no. 1, pp. 268–275, 2009.

[23] C. Mercier, R. Schneider, D. Billaud, J. C. Jumas, and J. Olivier-Fourcade, manuscript in preparation.

[24] K. Wan, S. F. Y. Li, Z. Gao, and K. S. Siow, "Tin-based oxide anode for lithium-ion batteries with low irreversible capacity," *Journal of Power Sources*, vol. 75, no. 1, pp. 9–12, 1998.